Full-Contact Domain Labeling: Identification of a Novel Phosphoinositide Binding Site on Gelsolin That Requires the Complete Protein†

Li Feng,‡,§ Marisan Mejillano,§,|| Helen L. Yin,*,|| Jian Chen,‡ and Glenn D. Prestwich*,‡

Department of Medicinal Chemistry, The University of Utah, Salt Lake City, Utah 84112, and Department of Physiology, The University of Texas Southwestern Medical Center at Dallas, Dallas, Texas 75229

Received May 1, 2000; Revised Manuscript Received November 1, 2000

ABSTRACT: Gelsolin, an actin and phosphoinositide binding protein, was photoaffinity labeled using a variety of benzophenone-containing phosphoinositide polyphosphate analogues. The N-terminal half and the C-terminal half of gelsolin showed synergy in the binding of phosphatidylinositol 4,5-bisphosphate [PtdIns(4,5)P_2]. Competitive displacement experiments with dibutyryl, dioctanoyl, or dipalmitoyl derivatives of PtdIns(4,5)P_2 suggested that, in addition to the inositol headgroup, a diacylglyceryl moiety was important for binding; these analogues also inhibited the gelsolin-severing activity of F-actin. In addition to the previously identified PtdIns(4,5)P_2 binding site in the N-terminal half of gelsolin, a new binding site was identified in the C-terminal half by mapping the photocovalently modified peptide fragments. Moreover, increasing concentrations of Ca^{2+} decreased the binding of the photolabile analogues to the C-terminal phosphoinositide binding site on gelsolin. A molecular model of the binding of PtdIns(4,5)P_2 within two folded repeats of gelsolin has been calculated using these data.

Actin structures in cells are dynamic and are affected by extracellular signals (*1*, *2*). The local assembly and disassembly of actin filaments allow remodeling of the cortical layer to form dynamic structures at cell surfaces. Studies from the last two decades have implicated gelsolin in actin cytoskeletal reorganizations (*3*, *4*). The consensus is that gelsolin (i) binds to the side of the actin fiber to sever the filament and dismantle the cytoskeleton, (ii) caps the fast growing filament barbed end to stop the growth of F-actin, and (iii) dissociates from the filament ends to allow actin polymerization from the uncapped ends. Gelsolin is activated by micromolar levels of Ca^{2+} and by slightly acidic conditions (*5*, *6*) but is inhibited by phosphoinositides (PtdInsP_ns)[1] (*7*).

Inhibition of gelsolin by PtdInsP_ns would allow selective growth of actin filaments by preventing gelsolin from severing filaments and also by releasing gelsolin from preformed filaments, in a process called "uncapping" (*4*). The study of the effects of PtdInsP_ns on gelsolin has been focused primarily on a single lipid, PtdIns(4,5)P_2. However, under certain conditions gelsolin also binds to PtdIns(3,4)P_2, and gelsolin−PtdIns(3,4,5)P_3 complexes have been isolated from osteoclasts (*8*).

Gelsolin alters PtdInsP_n turnover in vivo (*9*) and selectively affects inositol lipid remodeling in vitro, activating phosphatidylinositol 3-kinase (PI 3-K) (*8*) and phospholipase D (*10*) and inhibiting phospholipase Cγ (*9*, *11*) and phospholipase Cβ. These studies suggest a possible role for gelsolin in the modulation of lipid signaling events by interaction with the effector−PtdInsP_n complex or with the PtdInsP_n itself. Emerging evidence also supports a role for gelsolin in ion channel modulation (*12*) and as an effector in the signaling pathway from Rac GTPase to the cytoskeleton (*13*, *14*).

Direct binding assays showed that Ca^{2+} increases the affinity of gelsolin for PtdIns(4,5)P_2 over 7-fold (*5*), suggesting that Ca^{2+} may enhance PtdIns(4,5)P_2 binding by exposing cryptic sites and that gelsolin might use different PtdIns(4,5)P_2 binding sites in the presence and absence of Ca^{2+}. This would be analogous to the exposure of actin binding sites when Ca^{2+} binds to another part of the gelsolin molecule.

The interplay between different gelsolin domains is known to be important for Ca^{2+}-dependent activation of gelsolin binding to actin. Gelsolin has two tandem homologous halves, each of which contains a 3-fold segmental repeat (S1−S3 and S4−S6, respectively) (*4*). The two halves are functionally distinct. The N-half severs and caps actin filaments independent of Ca^{2+} concentration; in contrast, the C-half binds actin in a Ca^{2+}-dependent manner and acts as

† This work was supported by NIH Grants NS 29632 and GM 57705 to G.D.P. and GM 51112 to H.L.Y., and by an American Heart Association (Texas Associate) grant to H.L.Y.

* To whom correspondence should be addressed. Professor Glenn D. Prestwich, Department of Medicinal Chemistry, The University of Utah, 30 South 2000 East, Room 201, Salt Lake City, UT 84112-5820; phone: 801 585−9051; fax: 801 585−9053; e-mail: gprestwich@deans.pharm.utah.edu. Professor Helen L. Yin, Department of Physiology, University of Texas Southwestern Medical Center at Dallas, 5323 Harry Hines Boulevard, Dallas, TX 75390; phone: 214 648−7967; fax: 214 648−7891; e-mail: Helen.Yin@UTSouthwestern.edu.

‡ University of Utah.

§ These authors contributed equally to this work.

|| University of Texas.

[1] Abbreviations: BZDC, 4-benzoyldihydrocinnamoyl; LSC, liquid scintillation counter; NTCB, 2-nitro-5-thiocyano-benzoic acid; HPLC, high performance liquid chromatography; PI 3-K, phosphatidylinositol 3-kinase; PtdIns(3)P, phosphatidylinositol-3-phosphate; PtdIns(3,4)P_2, phosphatidylinositol 3,4-bisphosphate; PtdIns(3,4,5)P_3, phosphatidylinositol 3,4,5-trisphosphate; PtdIns(4,5)P_2, phosphatidylinositol 4,5-bisphosphate; PtdInsPns, phosphatidylinositol polyphosphates or phosphoinositides; PH, pleckstrin homology; PTH, phenylthiohydantoin.

10.1021/bi000996q CCC: $20.00
Published on Web 01/03/2001

a regulatory domain that inhibits severing by the N-half in the absence of Ca^{2+} (*4*). X-ray diffraction of full-length gelsolin crystals in the absence of Ca^{2+} showed that the N- and C-halves form a closed structure that precludes actin binding to any site, and the extreme C-terminus of the C-half appears to act as a "latch" to maintain the closed conformation (the "tail-latch" hypothesis) (*15*). Deletion of the C-terminal 23 amino acids of gelsolin (referred to as "tail") generated a completely Ca^{2+}-independent protein, establishing that the tail terminal residues act as a tail latch to confer Ca^{2+} regulation from the C-half to the N-half.

Much of the previous work on PtdIns(4,5)P_2 regulation of gelsolin has focused on the N-half, because PtdIns(4,5)P_2 inhibits severing of actin by the N-half. Furthermore, the N-half forms a EGTA−resistant 1:1 complex with actin, and PtdIns(4,5)P_2 is the only known agent that can dissociate the complex in vitro *(7)*. Using deletion mutagenesis and synthetic peptides, two putative N-half PtdInsP_n binding sequences (Gly^{132}−Phe^{149} and Arg^{161}−Arg^{172}) have been proposed (*16*−*18*). Each has an Arg- and Lys-rich consensus sequence that is likely to be important in the binding of the negatively charged headgroups of inositol lipids. This motif is found in a number of unrelated PtdInsP_n binding proteins, which do not have a recognizable pleckstrin homology (PH) domain. The tertiary structure of horse gelsolin crystallized in the absence of Ca^{2+} revealed that these two PtdIns(4,5)P_2 binding sites were spatially proximal and formed a pair of extended structures that could bind the same lipid headgroup simultaneously (*15*). Tuominen et al. reported that an intact gelsolin structure was needed for the efficient binding of PtdIns(4,5)P_2 (*19*), suggesting two possibilities. One explanation is that residues outside of the proposed PtdInsP_n-binding domains regulate PtdIns(4,5)P_2 binding. The alternative explanation is that the protein structure of the correctly oriented PtdIns(4,5)P_2 requires binding from multiple sites on gelsolin.

To address these possibilities, we have used photoactivatable analogues to map the PtdIns(4,5)P_2 binding sites in gelsolin. First, we provide evidence that efficient photocovalent attachment of photoactivatable triester analogues of PtdInsP_ns to gelsolin requires the full-length sequence of gelsolin. Second, we show that even though both C- and N-halves of gelsolin bind PtdIns(4,5)P_2, only the C-terminal half can be photoaffinity labeled. Indeed, labeling of the C-half is potentiated by the N-half, suggesting that optimal binding requires cooperative interactions between the two halves. Furthermore, labeling in intact gelsolin or the isolated C-half is decreased by micromolar Ca^{2+} concentrations. Third, we mapped the C-terminal PtdInsP_n cross-linking sites to an Arg/Lys-rich region, which resembles the consensus region found in the N-half, and to the C-terminal tail that interacts with the N-half PtdIns(4,5)P_2 binding region. Finally, we present a three-dimensional model for the interaction of gelsolin with PtdIns(4,5)P_2 in the absence of Ca^{2+}.

EXPERIMENTAL PROCEDURES

Chemicals. PtdInsP_n ligands and 4-benzoyldihydrocinnamoyl (BZDC)-modified affinity probes (Figure 1) were synthesized as described (*20*−*22*). Dibutyryl, dioctanoyl, and dipalmitoyl PtdInsP_ns were obtained from Echelon Research Laboratories Inc. (Salt Lake City, UT) and natural bovine brain PtdIns(4,5)P_2 was from Sigma Chemical Co. (St. Louis, MO) or from Calbiochem (San Diego, CA). All solutions were made in Nanopure water (ultrafiltered, distilled, and deionized). Proteases (sequencing grade) were obtained from Boehringer Mannheim (Indianapolis, IN). En^{3}Hance and XAR X-ray film were obtained from NEN Life Science Products (Boston, MA). Falcon plates (Becton Dickinson and Co., No. 3043/3072) were used for photolyzing the protein samples. Microcon concentrators were obtained from Amicon (Beverly, MA). All other reagents were obtained from Sigma.

Proteins. Human plasma gelsolin and its N- and C-half fragments were produced in *Escherichia coli* as described (*9*). The gelsolin construct lacking the C-terminal 23 amino acids, i.e., gelsolin (1−732), or simply GΔ23, was generated as described (*6*).

Gelsolin Severing Activity. Actin filament severing by gelsolin in the presence or absence of natural PtdIns(4,5)P_2 or the synthetic saturated acyl chain PtdIns(4,5)P_2 analogues (di-C_{16}, di-C_8, and di-C_4 was measured by monitoring the decrease in pyrene-actin fluorescence as F-actin filaments depolymerize upon dilution (*3*, *17*). Thus, a 2.0 μM solution of rabbit muscle G-actin labeled with *N*-(1-pyrenyl)iodoacetamide (Molecular Probes, Eugene, OR) was polymerized overnight in buffer B (25 mM Hepes, pH 7.2, 150 mM KCl, 2 mM $MgCl_2$, 0.5 mM ATP, 0.2 mM $CaCl_2$, and 0.5 mM β-mercaptoethanol). Polymerized actin was diluted to below 0.07 μM into buffer B containing 0.027 μM gelsolin, with or without PtdIns(4,5)P_2 micelles or soluble PtdIns(4,5)P_2 analogues prepared as described below. Fluorescence was recorded using a Perkin-Elmer LS-5 fluorescence spectrophotometer. The difference in the slope of the fluorescence curves with or without gelsolin was defined as the rate of severing and was assigned a 100% depolymerization rate. Depolymerization rates in the presence of gelsolin and PtdIns(4,5)P_2 and its synthetic analogue are expressed as a percentage of that observed with gelsolin alone.

Micelles of natural PtdIns(4,5)P_2 and the dipalmitoyl analogue were prepared by dissolving the lipids in water to a final concentration of 1 mM and then sonicating for 5 min at maximum power (Heat Systems Ultrasonics, Inc. model W185) as described (*5*). The dioctanoyl analogue was processed in the same manner, including the sonication, although it was water soluble; the dibutyryl analogue was simply dissolved in water.

Photoaffinity Labeling. In a typical photoaffinity labeling experiment (*23*−*25*), gelsolin (6 μg, 1.4 μM) or its fragment (3 μg, 1.4 μM) was mixed with 0.2 μCi of a given phosphoinositide probe (42.5 Ci/mmol, 0.1 μM). For peptide mapping, 20−40 μg of gelsolin or its C-terminal half was mixed with 1 μCi of [^{3}H]BZDC-*triester*-PtdIns(4,5)P_2 and unlabeled BZDC-*triester*-PtdIns(4,5)P_2 (protein/probe = 1:5) in labeling buffer (25 mM HEPES, 80 mM KCl, 1 mM EGTA, pH 7.0). The mixture was incubated for 15 min at 4 °C and then irradiated with long-wavelength UV light (RMR-3600, 350 nm, 1900 μW/cm^2) for 45 min at 4 °C.

For the competitive displacement assays using PtdIns and various acyl analogues of PtdIns(4,5)P_2, the stock phosphoinositide solutions were sonicated five times with bursts of 1 min each. Next, to 7.0 μg of gelsolin in the labeling buffer was added 0.55 μCi of [^{3}H]-BZDC-*triester*-PtdIns(4,5)P_2 (42.5 Ci/mmol) and a given phosphoinositide competitor at

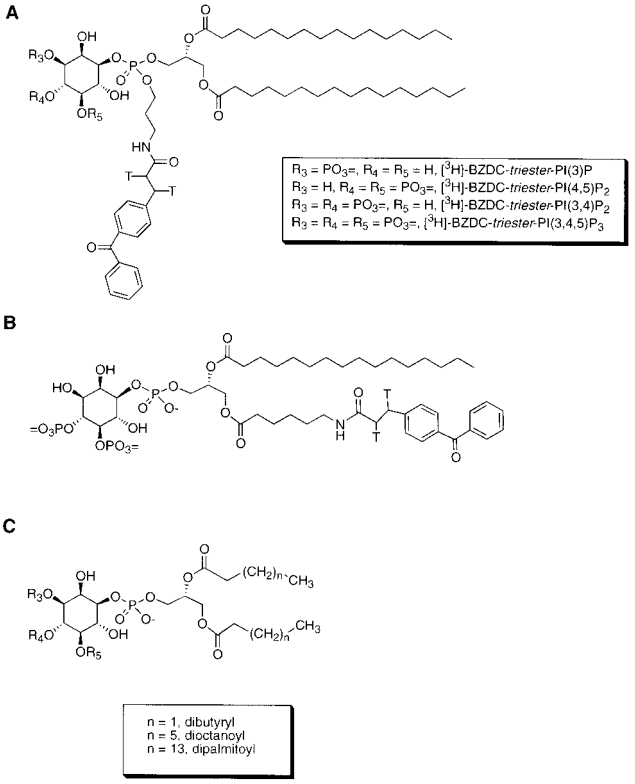

FIGURE 1: Phosphoinositide photoaffinity labels and competitors utilized in the photoaffinity labeling of gelsolin. Panel A, *triester* analogues; panel B, *acyl* analogue; panel C, three diacylglycerol chain length analogues used as competitors. Key: T = hydrogen or tritium.

0, 200, 500, and 1000 times molar excess relative to the photoaffinity probe. The mixture was incubated at 4 °C for 15 min and then irradiated for 45 min as described above.

CNBr Digestion of Gelsolin. The [^{3}H]BZDC-*triester*-PtdIns(4,5)P_2-labeled gelsolin was concentrated by a centrifugal evaporator (SpeedVac) to 50 μL, and 99% formic acid was added to make a 70% formic acid solution. CNBr (2000-fold molar excess) in 70% formic acid was then added. The mixture was incubated in the dark, under argon, at room temperature for 24 h, and then formic acid was removed in vacuo.

NTCB Digestion of Gelsolin. Lyophilized and [^{3}H]BZDC-*triester*-PtdIns(4,5)P_2-labeled gelsolin was mixed with 2-nitro-5-thiocyano-benzoic acid (NTCB, 100-fold molar excess) in 100 μL of 200 mM Tris/HCl, 7.5 M guanidium chloride, and 0.5 mM EDTA, pH 8.0. After stirring the sample for 1 h at room temperature, the pH was raised to 9.0 by addition of 1 M Tris base. The solution was incubated at 37 °C for 24 h, and the reaction was stopped by addition of 2-mercaptoethanol (NTCB/mercaptoethanol, 1:1). Guanidium chloride was removed by using a Microcon 3000 filter.

Reversed-Phase High Performance Liquid Chromatography (HPLC) of Chymotrypsin-Digested C-Half Gelsolin. [^{3}H]-BZDC-*triester*-PtdIns(4,5)P_2-labeled C-terminal half of gelsolin (40 μg, 50 μL) was mixed with 36 μg of solid urea to give an 8 M urea solution. The sample was warmed at 37 °C for 30 min and then 2.6 vol of water and 0.4 vol of digestion buffer (1 M ammonium bicarbonate) were added. $CaCl_2$ (1 M) was added to yield a 10 mM solution of Ca^{2+}. Chymotrypsin (6.0 μL, 1 mg/mL) was added, and the mixture was incubated at 37 °C for 5 h. The reaction was stopped by freezing at −20 °C. The chymotryptic fragments were separated by HPLC using a C_8 reversed-phase column (4.6 mm × 25 cm, Zorbax 300 SB−C-8), by elution at 1 mL/min with a gradient from 0 (solvent A) to 70% (solvent B) acetonitrile in water, with 0.1% TFA in solvent A and 0.085% TFA in solvent B. Eluted peptides were monitored by UV at 210 nm and collected automatically.

Reversed-Phase HPLC of Trypsin-Digested Gelsolin. [^{3}H]-BZDC-*triester*-PtdIns(4,5)P_2-labeled gelsolin was resolved on a sodium dodecyl sulfate polyacrylamide gel electrophoresis (SDS−PAGE) gel, and the gelsolin band was subjected to exhaustive in-gel tryptic digestion (0.5 μg/gel slice overnight). Tryptic peptides were separated by HPLC using a C_4 reversed-phase column using the gradient described above. The major peak of radioactivity was analyzed by MALDI-TOF mass spectroscopy and further fractionated by HPLC, using a 0 to 70% acetonitrile gradient containing 0.1% ammonium acetate in the eluting solvents. Fractions were collected and radioactivity was determined by liquid scintillation counting (LSC).

Sequencing of Radiolabeled Peptides. Radiolabeled peptides from reversed-phase HPLC separation were detected by LSC and the radioactive fractions were concentrated by SpeedVac. The peptides were sequenced by Dr. R. Schackmann (The University of Utah) and by Dr. C. Slaughter (University of Texas Southwestern Medical Center) by standard Edman degradation (*26*), and the phenylthiohydantoin (PTH)-amino acid derivatives were collected.

Glycine SDS−PAGE and Fluorography. Proteins were separated using a Mini-PROTEIN II dual slab cell system (Bio-Rad). Loading buffer (6×) was added, and the samples were denatured (100 °C, 5 min). The proteins were then separated by SDS−PAGE (*27*) at 150 V for 1.5 h. After electrophoresis, the gels were stained with 0.25% Coomassie-blue R-250 in 50% methanol and 10% acetic acid for 30 min and destained in 30% methanol and 10% acetic acid for 3 h.

For fluorography, the gels were impregnated with En^3-Hance for 45 min, precipitated with water, and miniaturized in 30% (w/v) PEG-2000. The gels were dried on 3 MM filter paper under vacuum (Welch Thomas Gelmaster) for 2 h at 60 °C. The dried gels were exposed to preflashed XAR-5 X-ray film for 1−2 weeks at −80 °C.

Tricine SDS−PAGE. Tricine gels (10 × 14 × 0.075 cm) were electrophoresed at 50 V for 20 h using a Hoefer 600 SE electrophoresis system and were composed of a small pore gel (16.5% T) overlaid by a 10% T, 3% C spacer gel and then by a 4% T, 3% C stacking gel (T, total concentration of both acrylamide and bisacrylamide; C, ratio of bisacrylamide to acrylamide). The protein bands were fixed in 50% methanol and 10% acetic acid for 30 min, stained with 0.25% Coomassie-blue Brilliant R in 10% acetic acid for 1 h and destained in 10% acetic acid for 2 h. For fluorography, the gels were treated as described above.

Molecular Modeling. The structure of horse gelsolin (dimer) was downloaded from Brookhaven Database (identification code 1D0N) into INSIGHTII (Biosym Technologies, version 97). Hydrogen atoms were added in the BUILDER module, and the structure was minimized by the OPTIMIZE command. BZDC-*triester*-PtdIns(4,5)P_2 was also composed in the BUILDER module, and its energy was minimized similarly. This ligand was manually docked to

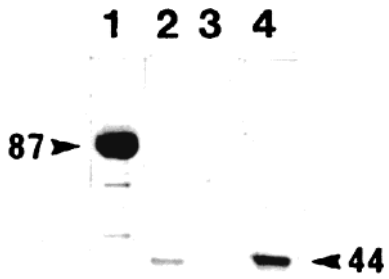

FIGURE 2: Synergistic effects of the N- and C-terminal halves of gelsolin on photoaffinity labeling. The fluorogram shows tritium-labeled protein bands for gelsolin and its fragments following photoaffinity labeling with [^{3}H]BZDC-*triester*-PtdIns(4,5)P_2. Key: full-length gelsolin (lane 1), C-terminal half of gelsolin (lane 2), N-terminal half of gelsolin (lane 3), and N-terminal half of gelsolin mixed with C-terminal half (lane 4).

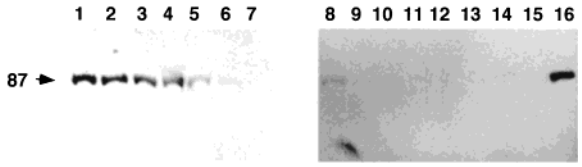

FIGURE 3: Fluorogram showing ligand specificity of gelsolin photoaffinity labeling by [^{3}H]BZDC-*triester*-PtdIns(4,5)P_2. Lanes 1 and 16, gelsolin labeled by [^{3}H]BZDC-*triester*-PtdIns(4,5)P_2 without competitors; lanes 2−4, competitions with PtdIns at 200-, 500-, and 1000-fold molar excess, respectively; lanes 5−7, competitions with natural PtdIns(4,5)P_2 at 200-, 500-, and 1000-fold molar excess, respectively; lanes 8−10, competitions with di-C_{16} PtdIns(4,5)P_2 at 200-, 500-, and 1000-fold molar excess, respectively; lanes 11−13, competitions with di-C_8 PtdIns(4,5)P_2 at 200-, 500-, and 1000-fold molar excess, respectively; lanes 14 and 15, competitions with di-C_4 PtdIns(4,5)P_2 at 200- and 500-fold molar excess, respectively.

the minimized gelsolin structure while monitoring the energy using the DOCKING module. Energy minimization was also carried out for the protein/ligand assembly using the OPTIMIZE command in the BUILDER module.

RESULTS

An Intact Structure of Gelsolin is Needed for Optimal Photoaffinity Labeling by PtdIns(4,5)P_2 Analogues. Full-length gelsolin, its N- and C-terminal halves were photoaffinity labeled with photolabile PtdIns(4,5)P_2 probes (Figure 2). The fact that full-length gelsolin was labeled by [^{3}H]-BZDC-*triester*-PtdIns(4,5)P_2 confirmed previous results that gelsolin effectively bound PtdIns(4,5)P_2 with high affinity. Another radioactive analogue of PtdIns(4,5)P_2, [^{3}H]*acyl*-BZDC-PtdIns(4,5)P_2, which has the BZDC photophore attached on the *sn*-1 acyl chain (*20*, *28*, *29*), did not label gelsolin at all (data not shown). The C-terminal half of gelsolin was photocovalently modified by [^{3}H]BZDC-*triester*-PtdIns(4,5)P_2 but, unexpectedly, the N-terminal half was not photolabeled. Interestingly, when the N-terminal and C-terminal halves of gelsolin were mixed in a 1:1 ratio, photolabeling of the C-half was increased.

The binding specificity of PtdIns(4,5)P_2 was demonstrated by competitive displacement with unlabeled ligands, using PtdIns as a negative control (Figure 3). Indeed, PtdIns (up to 1000-fold molar excess) showed little or no competitive displacement of the covalent modification of gelsolin by [^{3}H]-BZDC-*triester*-PtdIns(4,5)P_2. In contrast, all acyl chain analogues of PtdIns(4,5)P_2 showed efficient displacement of

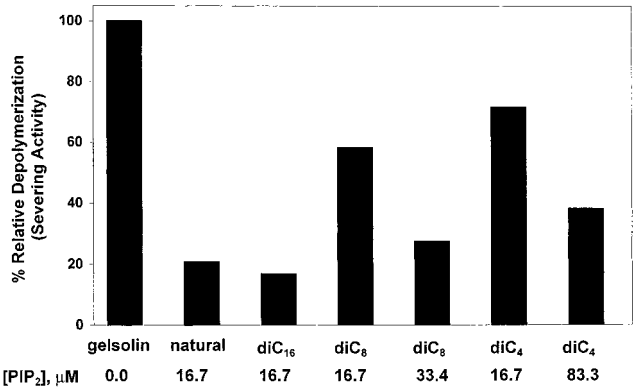

FIGURE 4: Inhibition of gelsolin severing activity by phosphoinositides. Actin filament severing by gelsolin was determined in the absence or presence of natural, di-C_{16}, di-C_8, and di-C_4 PtdIns(4,5)P_2 by measuring the rate of pyrene−actin depolymerization upon dilution with gelsolin. The rate of depolymerization in the absence of added phosphoinositide is defined as 100% on the *y*-axis.

photocovalent modification. In these experiments, the sonication of the lipid solutions was essential to deliver the phosphoinositides to the gelsolin in a fashion that permits competition to be observed. Natural, di-C_{16}, di-C_8, and di-C_4 PtdIns(4,5)P_2 each displaced the labeling efficiently at 500-fold excess and above, with the di-C_4 and di-C_8 PtdIns(4,5)P_2 analogues showing essentially complete competition at 200-fold excess. Thus, the shorter chain, water-soluble lipids appeared to have better access to gelsolin during the prolonged irradiation time, since they cannot form micelles that would effectively lower the amount of free lipid available for the displacement of the photoprobe.

Gelsolin-Mediated Depolymerization of Actin is Inhibited by Natural and Synthetic PtdIns(4,5)P_2. Actin filament severing by gelsolin (*17*) was measured in the absence or presence of natural, di-C_{16}, di-C_8, and di-C_4. Pyrene-actin fluorescence decreased as polymerized F-actin filaments depolymerize in the presence of gelsolin (*3*), and PtdIns(4,5)P_2 analogues inhibited this severing activity. Depolymerization rates in the presence of gelsolin and PtdIns(4,5)P_2 analogues are expressed relative to the rate for gelsolin alone. Figure 4 shows that natural and di-C_{16} PtdIns(4,5)P_2 are equipotent at 16.7 μM in reducing depolymerization to 20% of the gelsolin only severing activity. The di-C_8 analogue inhibited depolymerization but was slightly less potent, showing a reduction to 30% activity at 33.4 μM, while the di-C_4 analogue showed a reduction to 40% activity at 83.3 μM. Interestingly, the radioinert photoaffinity analogue, BZDC-*triester*-PtdIns(4,5)P_2, showed a modest reduction of depolymerization to 50% activity at 25 μM (data not shown), demonstrating that the phosphotriester photoaffinity probe can bind in a physiologically relevant manner despite the steric congestion introduced at the P-1 phosphate.

Ca^{2+} Effects. A number of physicochemical measurements indicate that gelsolin undergoes a global conformation change in the presence of Ca^{2+}. We therefore examined the effects of Ca^{2+} on the labeling of gelsolin by [^{3}H]BZDC-*triester*-PtdIns(4,5)P_2. Ca^{2+} at either 0.2 mM (data not shown) or 36 μM (Figure 5) inhibited the labeling of gelsolin and the gelsolin C-half. These results suggest that the Ca^{2+} induced changes in full-length gelsolin and the gelsolin C-half conformations preclude efficient photoaffinity labeling by [^{3}H]BZDC-*triester*-PtdIns(4,5)P_2. The decrease in photo-

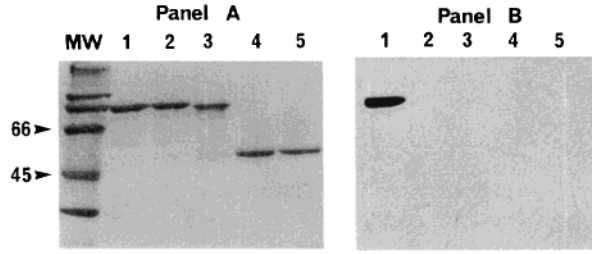

FIGURE 5: Effect of Ca^{2+} on labeling of gelsolin by [^{3}H]BZDC-*triester*-PtdIns(4,5)P_2. Panel A, Coomassie-blue stained proteins; panel B, fluorogram. Lane 1, labeling of full-length gelsolin in the absence of Ca^{2+}; lanes 2−5, labeling in the presence of 36 μM Ca^{2+}. Full-length gelsolin is in lane 2, GΔ23 is in lane 3, N-terminal half is in lane 4, and the C-terminal half is in lane 5.

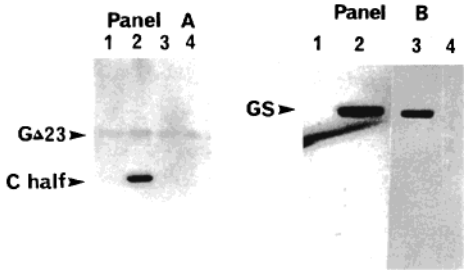

FIGURE 6: Panel A: The synergistic effects of GΔ23 and the C-terminal half of gelsolin. Fluorogram showing labeling of GΔ23 and the C-terminal half were labeled by [^{3}H]BZDC-*triester*-PtdIns-(4,5)P_2. Lane 1, GΔ23 mixed with the C-terminal half in the presence of 0.2 mM Ca^{2+}; lane 2, GΔ23 mixed with the C-terminal half of gelsolin in the absence of Ca^{2+}; lane 3, GΔ23 in the presence of 0.2 mM of Ca^{2+}; lane 4, GΔ23 in the absence of Ca^{2+}. Panel B: Fluorogram showing labeling of full-length gelsolin by 3-phosphorylated phosphoinositide analogues. Lane 1, [^{3}H]BZDC-*triester*-PtdIns(3)P; lane 2, [^{3}H]BZDC-*triester*-PtdIns(3,4)P_2; lanes 3 and 4, [^{3}H]BZDC-*triester*-PtdIns(3,4,5)P_3 in the absence (lane 3) and presence (lane 4) of 0.2 mM Ca^{2+}. The diagonal line is an artifact.

covalent modification of the C-half by Ca^{2+} is consistent with our previous finding that Ca^{2+} reduced the affinity of gelsolin for PtdIns(4,5)P_2 (*9*). However, the decrease in photolabeling of gelsolin is not consistent with our previous finding that Ca^{2+} increases binding affinity of gelsolin for PtdIns(4,5)P_2. This seemingly paradoxical behavior will be discussed below.

Ca^{2+} regulation of the gelsolin and gelsolin C-terminal half is critically dependent on the presence of its C-terminal tail (*6*). Deletion of the C-terminal 23 amino acids to give GΔ23 resulted in a protein that could sever actin in the absence of Ca^{2+} and allowed the C-terminal half to bind to actin in the absence of Ca^{2+}. If the Ca^{2+}-free conformation is required for optimal photoaffinity labeling, we predict that GΔ23 would have decreased labeling. This is confirmed by our finding that GΔ23 was not detectably labeled by [^{3}H]-BZDC-*triester*-PtdIns(4,5)P_2 (Figure 6, panel A). Nonetheless, GΔ23 was still able to enhance the labeling intensity of the C-terminal half when the two proteins were mixed in a 1:1 ratio (Figure 6, panel A). In contrast, the labeling of GΔ23 was not significantly enhanced by the C-terminal half.

Gelsolin Binds to 3′-Phosphorylated Phosphoinositides. Photocovalent modification of gelsolin with 3′-phosphorylated phosphoinositide affinity probes was also examined. Gelsolin was labeled by [^{3}H]BZDC-*triester*-PtdIns(3,4,5)P_3 with the same efficiency as observed with the [^{3}H]BZDC-*triester*-PtdIns(4,5)P_2 probe (Figure 6, panel B); moreover,

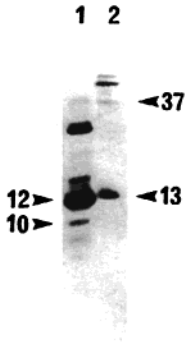

FIGURE 7: Fluorogram illustrating the chemical digestion of gelsolin labeled by [^{3}H]BZDC-*triester*-PtdIns(4,5)P_2. Lane 1, digestion with CNBr; lane 2, digestion with NTCB.

a 200-fold excess of di-C_8 PtdIns(3,4,5)P_3 completely displaced the covalent modification (data not shown). While [^{3}H]BZDC-*triester*-PtdIns(3)P did not photolabel gelsolin, [^{3}H]BZDC-*triester*-PtdIns(3,4)P_2 did label gelsolin with an efficiency similar to that observed for [^{3}H]BZDC-*triester*-PtdIns(3,4,5)P_3 and [^{3}H]BZDC-*triester*-PtdIns(4,5)P_2 (Figure 6, panel B).

Active Binding Site Mapping. To further explore the binding mechanism between gelsolin and phosphoinositides, the [^{3}H]BZDC-*triester*-PtdIns(4,5)P_2-modified sites were identified using several independent approaches. First, photoaffinity-labeled gelsolin was subjected to chemical digestion with two different reagents. The polypeptide fragments were analyzed by tricine SDS−PAGE and fluorography (Figure 7) and compared with the digestion patterns predicted by MacVector. The digestion of the [^{3}H]BZDC-*triester*-PtdIns-(4,5)P_2-labeled gelsolin by NTCB (which cleaves at the N-terminal side of Cys residues) generated a major 12.7 kDa (assigned as Ser^{645}−Ala^{755}) labeled band and a minor 37 kDa (likely Cys^{304}−Ala^{644}) labeled band on the fluorogram. Cyanogen bromide digestion of gelsolin, which cleaved at the C-terminal side of Met residues, generated three fragments: a 12-kDa radioactive fragment (assigned as Ile^{518}−Met^{635}) as well as 10.2 and 10.6 kDa fragments of interest.

Second, to further localize the covalently modified regions, the [^{3}H]BZDC-*triester*-PtdIns(4,5)P_2-labeled gelsolin C-terminal half and full-length gelsolin were digested to give smaller polypeptides using chymotrypsin and trypsin, respectively. The peptides were separated using reversed-phase HPLC. Three major radioactive fractions were obtained after fractionation of the chymotrypsin-digested gelsolin C-terminal half (Figure 8, panel A). The fraction with the highest radioactivity (peak 3) was unreacted BZDC-*triester*-PtdIns-(4,5)P_2 as determined in a control experiment. The two peptidic radioactive fractions were concentrated and sequenced by Edman degradation (10 cycles each). Two proteolytic peptide fragments could be assigned as Arg^{599}−Trp^{615} and Ser^{742}−Ala^{755}. The placement of these two chymotryptic radioactive peptides into larger labeled fragments is consistent with the chemical digestion studies.

HPLC fractionation of the tryptic fragments of [^{3}H]BZDC-*triester*-PtdIns(4,5)P_2-labeled full-length gelsolin yielded several radiolabeled fractions; the major peak accounted for 47% of total TCA-precipitable radioactivity loaded onto the column (Figure 8, panel B). MALDI-TOF mass spectroscopic analysis showed that this peak contained two peptides with *m*/*z* 1852 and 2141. Edman degradation suggested the

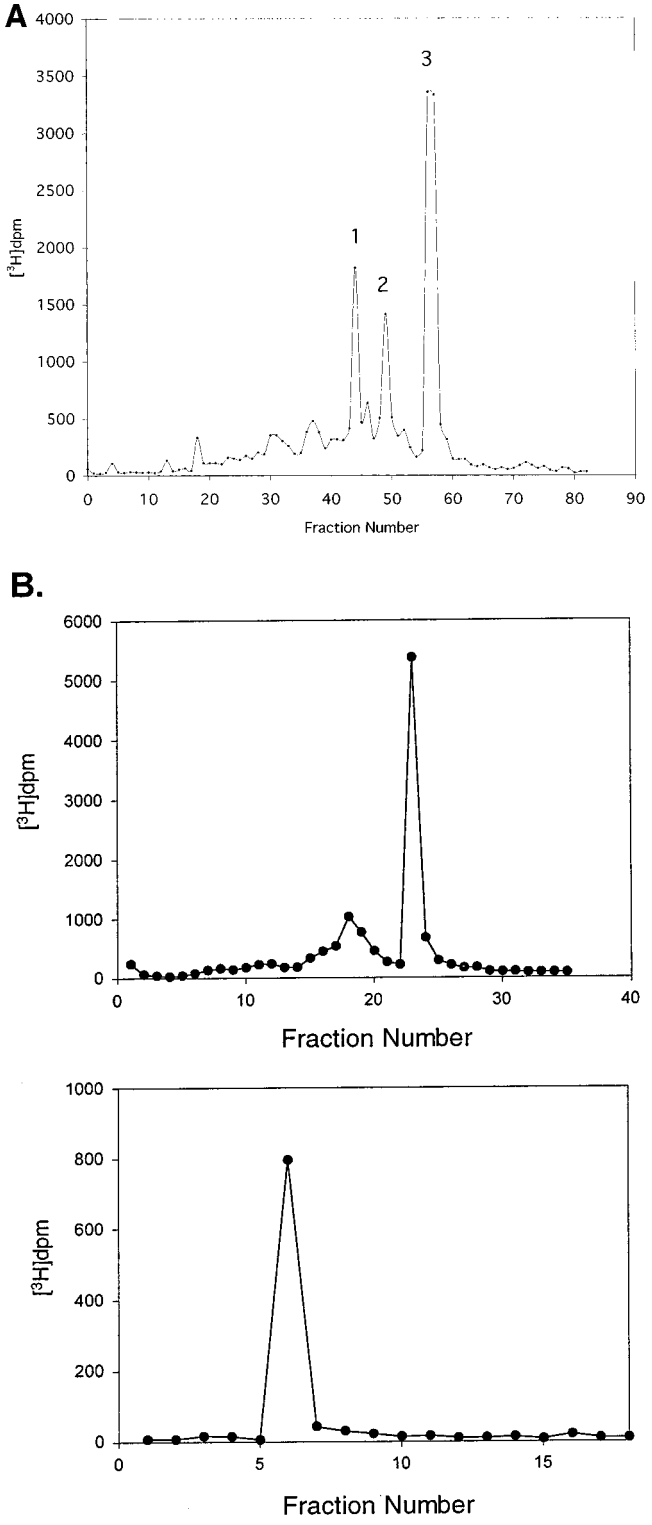

FIGURE 8: Analysis of radiolabeled gelsolin peptides. Panel A, HPLC separation of chymotrypsin-digested C-terminal half of gelsolin. Panel B, trypsin-digested full-length gelsolin from in-gel digestion using an unbuffered aqueous system (top). The major peak was rechromatographed by HPLC using an ammonium acetate buffer system (bottom).

presence of two polypeptides with Gly^{620} and Gln^{722} as their respective N-terminal residues. When this sample was refractionated by HPLC using a different mobile phase, a single radioactive peak was recovered (Figure 8, panel B). Edman degradation showed evidence for a single peptide, spanning Ala^{600}−Arg^{625}. This tryptic fragment overlaps with the independently identified Arg^{599}−Trp^{615} chymotryptic fragment and Ile^{518}−Met^{635} CNBr fragment. It has two basic residues (Lys^{621} and Arg^{625}) and is contiguous with a downstream sequence that partially matches the PtdIns(4,5)-P_2-binding consensus sequence identified earlier at the gelsolin N-terminal half (*16*−*18*).

Molecular Modeling. To explore which residues of gelsolin are necessary for binding to phosphoinositides, molecular modeling based on the crystal structure of horse plasma gelsolin, with BZDC-*triester*-PtdIns(4,5)P_2 as the ligand, was carried out. Horse plasma gelsolin crystallized as a dimer (1458 residues) with 350 structural water molecules (*15*). The N-terminus (*1*−*26*) of this protein was not resolved. The coordinates of the structure were downloaded from Protein Data Bank and visualized by INSIGHTII, the VIEWER module.

Hydrogen atoms were added to the gelsolin structure, and the dimer was minimized using the BUILDER module/OPTIMIZE command. The BZDC-*triester*-PtdIns(4,5)P_2 molecule (bearing four negative charges) was assembled in the BUILDER module, and its energy was minimized by the OPTIMIZE command. The BZDC-*triester*-PtdIns(4,5)-P_2 molecule was manually docked into the minimized structure of gelsolin, between the regions of the radioactive peptides identified by peptide mapping and the proposed Lys/Arg-rich regions.

To simplify the docking and minimization procedures, only domains that have possible contacts with the small ligand were selected to constitute an assembly with BZDC-PtdIns-(4,5)P_2. The assemblies were again minimized. That is, domains S1, S2, and S6 were assembled with BZDC-*triester*-PtdIns(4,5)P_2 and domains S3, S5, and S6 were assembled with another BZDC-*triester*-PtdIns(4,5)P_2 molecule. During the energy minimization process, the BZDC-*triester*-PtdIns-(4,5)P_2 molecules moved away from the original docking sites and settled into different locations in which the four negatively charged oxygens formed electrostatic interactions with the Lys/Arg residues. Importantly, the carbonyl of the benzophenone was still located within bonding range of the identified radioactive peptides. For each binding site, there were at least three hydrogen bonds predicted (Figure 9).

In the assembly of domains S1, S2, and S6 with BZDC-*triester*-PtdIns(4,5)P_2, the residues Lys^{166}, Arg^{168}, and Arg^{169} were shown to be within 10 Å of the four negative charges on the headgroup of BZDC-*triester*-PtdIns(4,5)P_2. Phe^{208} (Tyr^{208} in human plasma gelsolin), Leu^{211}, Arg^{748}, and Leu^{753} were predicted to form four hydrogen bonds with the BZDC-*triester*-PtdIns(4,5)P_2 molecule. After minimization, the carbonyl oxygen is 2.99 Å from one of the β-hydrogens of Leu^{753}, implicating this site in covalent modification during the photolabeling reaction (*30*). In the assembly of domains S3, S5, and S6 with BZDC-*triester*-PtdIns(4,5)P_2, the residues Lys^{631}, Lys^{633}, Lys^{634}, Arg^{542}, Arg^{625}, and Arg^{629} were proximal to the negative charges of the ligand. Glu^{587}, Asp^{632}, and Gly^{582} were predicted to be involved in hydrogen bonding with BZDC-*triester*-PtdIns(4,5)P_2. Similarly, after minimization, one β-hydrogen of Ala^{606} is within 3 Å of the carbonyl oxygen in the BZDC-*triester*-PtdIns(4,5)P_2 molecule. Thus, Ala^{606} was probably modified by the ligand during photoaffinity labeling.

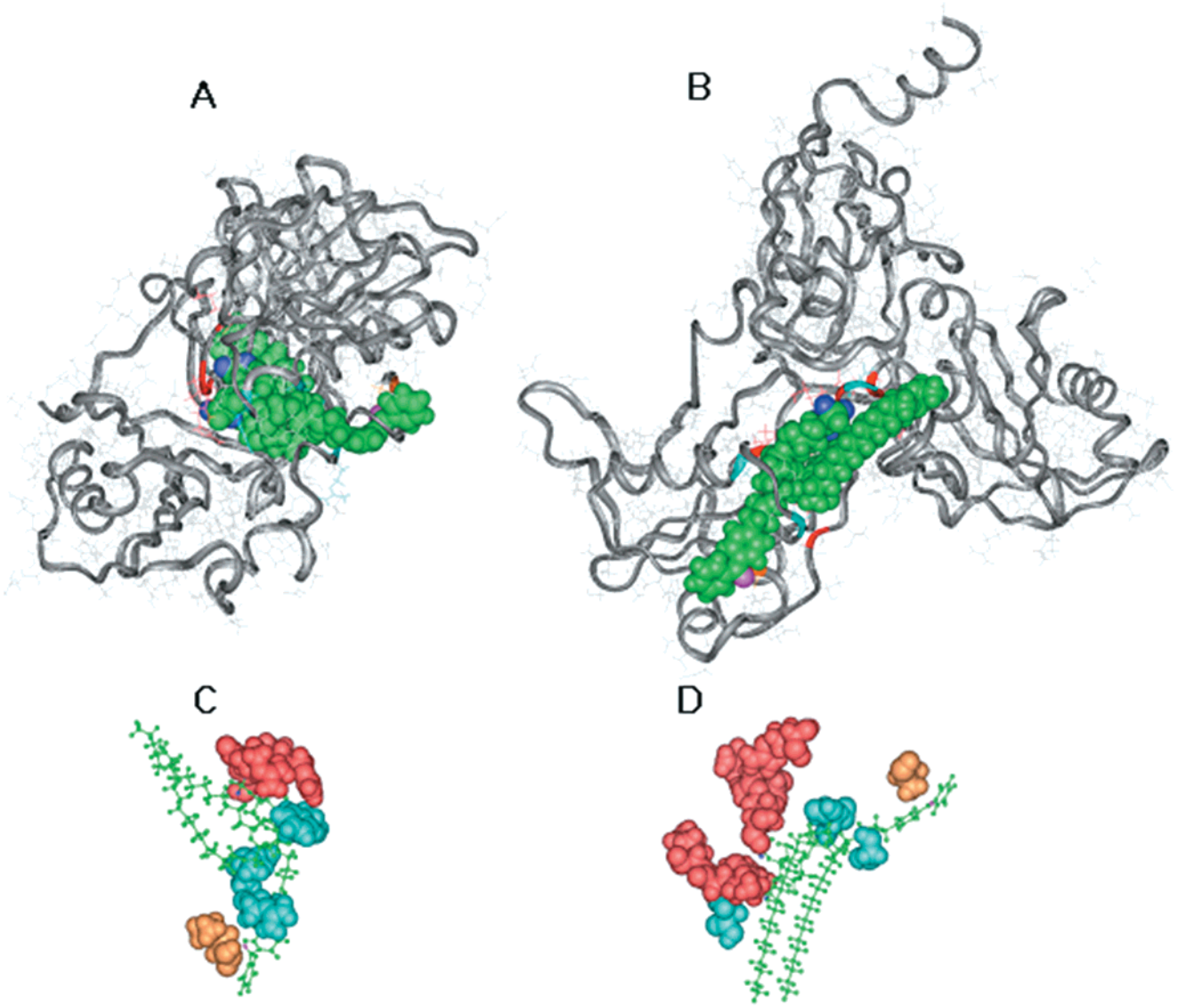

FIGURE 9: Molecular modeling of horse plasma gelsolin with BZDC-PtdIns(4,5)P_2 as the ligand. Panel A, domains S1, S2, and S6 with BZDC-PtdIns(4,5)P_2. Panel B, domains S3, S5, and S6 with BZDC-PtdIns(4,5)P_2. Panel C, a close-up model of PtdIns(4,5)P_2 and the residues in domains S1, S2, and S6 involved in the binding. Panel D, a close-up model of PtdIns(4,5)P_2 and the residues in domains S3, S5, and S6 involved in the binding. BZDC-PtdIns(4,5)P_2 is green. The carbonyl oxygen of BZDC is magenta and the four oxygens bearing negative charges are blue. Lys and Arg residues (Lys^{166}, Arg^{168}, and Arg^{169} in panels A and C; Lys^{631}, Lys^{633}, Lys^{634}, Arg^{542}, Arg^{625}, and Arg^{629} in panels B and D, respectively) proximal to the ligand are shown in red. Residues (Phe^{208}, Leu^{211}, Arg^{748}, and Leu^{753} in panels A and C, Glu^{587}, Asp^{632}, and Gly^{582} in panels B and D, respectively) involved in hydrogen bonding are turquoise. The covalently modified residues are yellow (Leu^{753} and Ala^{606}, respectively, in panels A and C and panels B and D).

DISCUSSION

The availability of photoactivatable PtdInsP_n analogues has enabled the identification and characterization of a wide variety of PtdInsP_n binding proteins (*20*, *30*, *31*). These ligands have proven to be extremely site-specific, and the photophore is positioned on a tethered linkage, thus avoiding substantial interference with the important binding interactions. The BZDC-PtdInsP_n analogues have found extensive applications in the modification and identification of the active sites of proteins that recognize Ins(1,4,5)P_3 (*32*) Ins(1,3,4,5)P_4 (*33*, *34*), InsP_6 (*34*), PtdIns(4,5)P_2 (*29*), or PtdIns(3,4,5)P_3 (*23*, *35*) as ligands.

The observation that [^{3}H]BZDC-*triester*-PtdIns(4,5)P_2 specifically photolabeled gelsolin while the [^{3}H]BZDC-*acyl*-PtdIns(4,5)P_2 probe failed to label gelsolin suggests that the headgroup of the inositol lipid is very important in determining the binding affinity. Unlike the PH domains (e.g., phospholipase C δ1 PH and Btk-PH), gelsolin binding to PtdIns(4,5)$_2$ is dependent not only on the phosphorylated headgroups but also on the presence of the diacylglyceryl moiety. This is illustrated by the efficient displacement of photolabeling by each of the PtdIns(4,5)P_2 acyl chain analogues, particularly the water-soluble, non-micelle-forming di-C_8 and di-C_4 PtdIns(4,5)P_2 derivatives. This observation is reinforced by the failure of the headgroup alone (Ins(1,4,5)P_3) to displace photolabeling, and is further supported by the failure of [^{3}H]BZDC-Ins(1,4,5)P_3 to label the protein efficiently (data not shown). Apparently, hydrophobic interactions of diacyl chains within the three-dimensional binding site are an important component of the binding interaction. This result contrasts with the profilin-PtdIns(4,5)P_2 interaction, in which [^{3}H]BZDC-Ins(1,4,5)P_3 was the label of choice. A pincer-like interaction between

the base-rich C-terminal helix and the hydrophobic N-terminal helix was identified as the PtdIns(4,5)P_2 binding site (*29*).

In aqueous solutions, natural (*sn*-1-*O*-stearoyl, 2-arachidonoyl) PtdIns(4,5)P_2 tends to form micelles at concentrations in excess of 15 μM (*36*, *37*). Use of PtdInsP_n derivatives above their critical micelle concentration results in formation of micelles that limit the availability of "free" ligand for interaction with the binding sites of the protein and may explain why natural and di-C_{16} PtdIns(4,5)P_2 were slightly less potent competitors relative to the water-soluble di-C_8 and di-C_4 analogues of PtdIns(4,5)P_2 in competitive displacement of the [^{3}H]BZDC-*triester*-PtdIns(4,5)P_2 labeling of gelsolin (Figure 3). The photoaffinity labeling results are further supported by the inhibition of gelsolin-mediated F-actin depolymerization by natural, di-C_{16}, di-C_8, di-C_4 and BZDC-PtdIns(4,5)P_2, which are listed in rank order of potency (Figure 4).

In the study of PtdInsP_n binding proteins, PtdIns(4,5)P_2 is always considered a central player (*38*), since it is the precursor of the second messengers Ins(1,4,5)P_3 and PtdIns(3,4,5)P_3 and also one of the most abundant inositol lipids. However, the involvement of the PI 3-K products (*39*), such as PtdIns(3,4)P_2 and PtdIns(3,4,5)P_3, in protein trafficking and regulation of cytoskeletal remodeling, is also well-documented. For example, we report herein that [^{3}H]BZDC-*triester*-PtdIns(3,4,5)P_3 and PtdIns(3,4)P_2 probes labeled gelsolin with efficiencies equivalent to that of the PtdIns(4,5)P_2 probe. In contrast, the α-COP subunit of the bovine liver COPI coatomer heteroheptamer was selectively labeled by [^{3}H]BZDC-*triester*-PtdIns(3,4,5)P_3 but not by other PtdInsP_n analogues (*23*). It is believed that all the barbed ends of actin filaments are capped by gelsolin and other capping proteins in resting cells and that gelsolin is uncapped by PtdIns(4,5)P_2 (*4*). Activation of the PI 3-K pathway may similarly uncap the F-actin and promote filament growth when the levels of PtdIns(3,4,5)P_3 or PtdIns(3,4)P_2 are increased. Ca^{2+} is a potent activator of gelsolin in binding to and severing actin, while PtdInsP_ns participate in a counterbalancing role of gelsolin−actin modulation. Additional studies will be required to determine which PtdInsP_n is the predominant regulator of gelsolin in vivo.

Gelsolin was labeled by [^{3}H]BZDC-*triester*-PtdIns(4,5)P_2 in the absence of Ca^{2+} but not in its presence. High concentrations of divalent cations such as Ca^{2+} can induce an extended structure in inositol lipids by bridging their phosphate groups (*37*) and thus reduce he solution availability of probes to the binding proteins. This is unlikely to occur at the concentration (36 μM Ca^{2+}) used in this study. Probably, the effects of low Ca^{2+} concentrations on PtdInsP_n labeling of the gelsolin C-half site have physiological significance. Micromolar levels of Ca^{2+} have been shown to alter the interaction of gelsolin with PtdIns(4,5)P_2. Consistent with the present result, 100 μM Ca^{2+} decreased the enhancement of fluorescence emission of NBD-labeled PtdIns(4,5)P_2 by gelsolin (*19*). However, direct binding studies also demonstrated that micromolar Ca^{2+} increased the apparent affinity of gelsolin for PtdIns(4,5)P_2 but decreased the affinity of each gelsolin half (*5*). Taken together, these results suggest that gelsolin may have multiple PtdIns(4,5)P_2 binding sites and that the two halves cooperate to generate the PtdIns(4,5)P_2 binding characteristics of full-length gelsolin. The difference between photoaffinity labeling and direct binding may reflect the behavior of different PtdIns(4,5)P_2 binding sites.

The photoaffinity labeling results described herein suggest that the N- and C-terminal halves cooperate to bind PtdIns(4,5)P_2 in the absence of Ca^{2+}. The C-terminal half was photoaffinity labeled in isolation, but labeling was increased substantially in the presence of the N-terminal half, even though the N-terminal half was not labeled. Previous assays demonstrated that the C-terminal can bind PtdIns(4,5)P_2, although with a lower affinity (*5*). Since the N-terminal half and C-terminal half form a compact structure only in the absence of Ca^{2+}, we suggest that the interaction between the N- and the C-terminal halves promotes PtdIns(4,5)P_2 binding.

The three-dimensional structure of gelsolin suggests that the N- and C-terminal halves in the intact molecule have multiple sites of interaction in the absence of Ca^{2+}. Yet whether N- and C-terminal halves bind to each other when present as separate entities in dilute solution has not been determined experimentally. Nonetheless, this appears to be likely; Pope et al. found that when gelsolin is proteolytically cleaved at the junction between the first segment and the remaining five gelsolin segments, the fragments associate with each other in the absence of Ca^{2+} (*40*). The requirement for N- and C-terminal half interactions for photoaffinity labeling to occur was confirmed by deleting the C-terminal gelsolin tail, which has been strongly implicated in the communication of Ca^{2+} information from the C-terminal half to the N-terminal half (the tail-latch hypothesis) and in the maintenance of the gelsolin C-terminal half in an inactive conformation (with respect to interaction with actin) in the absence of Ca^{2+} (*6*, *41*). Deletion of the C-terminal 23 residues (GΔ23) rendered full-length gelsolin and the gelsolin C-half completely Ca^{2+}-independent in their interactions with actin. Moreover, GΔ23 could not be photoaffinity labeled by [^{3}H]BZDC-*triester*-PtdIns(4,5)P_2.

The absence of labeling of GΔ23 is consistent with earlier predictions and may be attributed to a combination of factors. First, peptide mapping studies indicated that [^{3}H]BZDC-*triester*-PtdIns(4,5)P_2 modifies a site within the C-terminal 23 amino acids, and these 23 residues are in proximity to the two previously identified sites in the S2 domain. Deletion of this site would partially account for the loss of labeling.

Second, the lack of labeling of the second potential cross-linking site, which includes the peptide sequences spanning Arg^{599}−Trp^{615} and Gly^{600}−Lys^{625}, could be explained by the conversion of the gelsolin C-terminal half after tail deletion from a Ca^{2+}-free conformation to a Ca^{2+}-activated conformation. We recently found that Ca^{2+} induces a global conformational change in gelsolin C-terminal half (*42*) and that deletion of the 23 residue tail allowed the gelsolin C-terminal half to bind actin even in the absence of Ca^{2+} (*6*). Third, deletion of the tail also disrupts the interaction between the N- and C-terminal halves (tail unlatching) and therefore eliminates the cooperative aspect of the cross-linking.

The identification of two cross-linked regions allows us to predict via molecular modeling (Figure 9) how PtdIns(4,5)P_2 binds gelsolin in the absence of Ca^{2+}, by using the crystal structure of Ca^{2+}-free gelsolin (*15*). As shown schematically in Figure 10, the photoaffinity labeled gelsolin

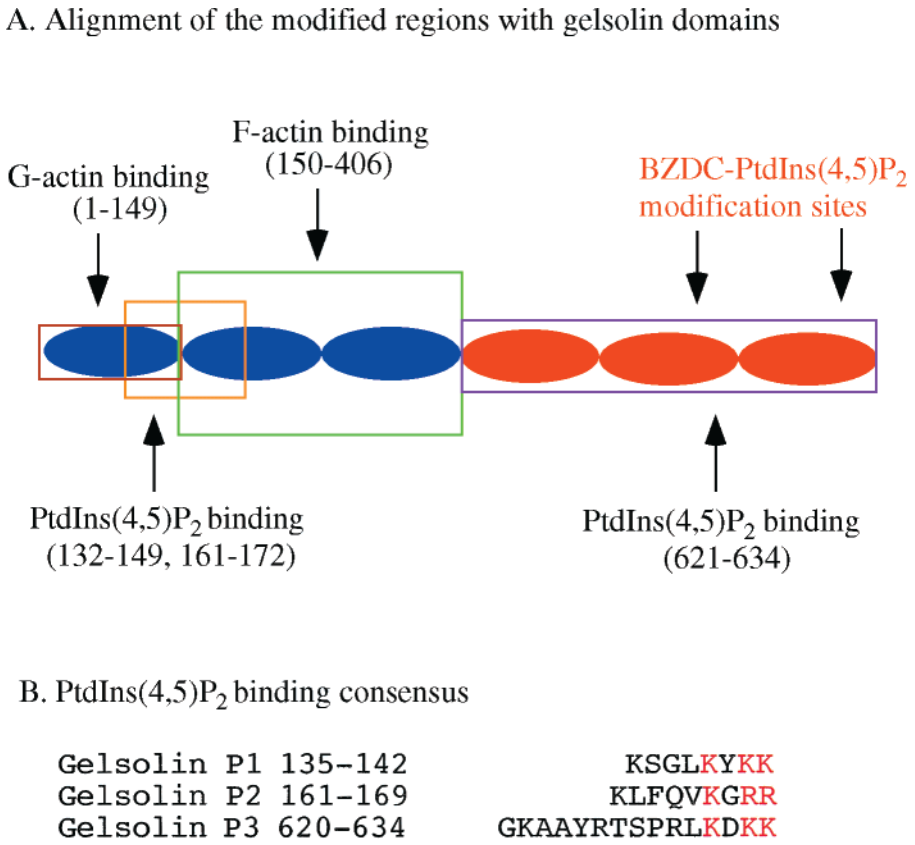

FIGURE 10: The binding sites of actin and PtdIns(4,5)P_2 in gelsolin. Panel A, alignment of modified regions with gelsolin domains. Panel B, PtdIns(4,5)P_2 binding consensus sequences. P1 and P2 were previously identified PtdIns(4,5)P_2 binding peptides, which probably are clustered together to form a single PtdIns(4,5)P_2 binding site at the gelsolin S1 and S2 interface. P3 is the newly identified PtdIns(4,5)P_2 binding site at the interface between S5 and S6. Basic residues that can potentially bind the PtdIns(4,5)P_2 inositide headgroup are shown in red.

peptide (Ser^{742}−Ala^{755}) and basic residues Lys^{166}, Arg^{168}, and Arg^{169}, which are within the previously identified binding region (P2), enclose a cavity that could accommodate an inositol headgroup with a pendant diacylglyceryl moiety. Yet the strong binding is not just limited to those residues. Tyr^{208}, Leu^{211}, Arg^{748}, and Leu^{753} are all located proximal to this cavity and could contribute significantly by hydrogen bonding as predicted by the molecular modeling. Lys^{212} is also within range for electrostatic interactions, but these interactions would require experimental verification.

The second covalently modified region (spanning residues 599 to 625) is proximal to another region rich in basic residues (Lys^{621}−Lys^{634}) (Figure 10, panel B). Since the region spanning Gly^{620} to Lys^{632} partially matches the previously identified N-terminal half PtdIns(4,5)P_2 binding consensus (P1 and P2), we propose that it is involved in PtdIns(4,5)P_2 binding. We have designated this as P3. As with the P1 and P2 sequences, the P3 sequence is located at a linker region between the S5 and the S6 domains. It has been hypothesized that PtdIns(4,5)P_2 binding to the S1−S2 linker inhibits the local rearrangements that must occur in the linker region to permit S2 and S1 to bind two actins simultaneously (*43*). Our finding that the C-terminal half PtdIns(4,5)P_2 binding site is also located in a linker suggests that this hypothetical mechanism for PtdIns(4,5)P_2 inhibition of gelsolin may have some merit. Similar to the C-terminal tail binding site, hydrogen bond donors, Glu^{587} and Asp^{632}, as well as the backbone hydrogen bond acceptor Gly^{582}, provide a hydrophilic environment for the inositol phosphate ring. Lys^{631}, Lys^{633}, Lys^{634}, Arg^{542}, Arg^{625}, and Arg^{629} comprise an array of basic residues that stabilize interactions with the bisphosphate. Thus, the labeling data reported herein and the predicted molecular model suggest that the active binding sites for PtdIns(4,5)P_2 in gelsolin are not located in the tight core of the α-helices or β-sheets; instead, these are located on loops or on the surfaces of secondary structures, allowing the incorporation of amphiphilic phosphoinositides at the interface of lipid/protein/water. Such a model is consistent with the model for the profilin−PtdIns(4,5)P_2 interaction (*29*) and with the proposed interaction of the "flounder-like" phosphoinositide 4-kinase with its membrane-bound ligand (*44*).

In conclusion, we have identified novel binding sites of PtdIns(4,5)P_2 in the C-terminal half of gelsolin and showed that an intact structure of gelsolin is required for efficient binding to phosphoinositides. The physiological functions of gelsolin appear to be regulated by its binding to Ca^{2+}, PtdIns(4,5)P_2, and PtdIns(3,4,5)P_3, and the regulation depends on the type of extracellular stimulation.

ACKNOWLEDGMENT

We thank Echelon Research Laboratories Inc. (Salt Lake City, UT; www.echelon-inc.com) for the gift of the soluble phosphoinositides employed in the competition experiments. We thank Dr. C. Slaughter and C. Moomaw (University of Texas Southwestern Medical Center), and Dr. R. Schackmann (The University of Utah) for assistance with HPLC and MALDI-TOF analysis and with amino acid sequencing.

REFERENCES

1. Machesky, L. M., and Insall, R. H. (1998) *J. Cell Biol. 146*, 267−272.
2. Yin, H. L., and Stull, J. T. (1999) *J. Biol. Chem. 274*, 33179−33182.
3. Kwiatkowski, D. J., Janmey, P. A., and Yin, H. L. (1989) *J. Cell Biol. 108*, 1717−1726.
4. Sun, H., Yamamoto, M., Mejillano, M., and Yin, H. (1999) *J. Biol. Chem. 274*, 33179−33182.
5. Lin, K. M., Wenegieme, E., Lu, P. J., Chen, C. S., and Yin, H. L. (1997) *J. Biol. Chem. 272*, 20443−20450.
6. Lin, K. M., Mejillano, M., and Yin, H. L. (2000) *J. Biol. Chem. 275*, 27746−27752
7. Janmey, P. A., and Stossel, T. P. (1987) *Nature 325*, 362−364.
8. Chellaiah, M., Fitzgerald, C., Alvarez, U., and Hruska, K. (1998) *J. Biol. Chem. 273*, 11908−11916.
9. Sun, H. Q., Lin, K. M., and Yin, H. L. (1997) *J. Biol. Chem. 138*, 811−820.
10. Steed, P. M., Nagar, S., and Wennogle, L. P. (1996) *Biochemistry 35*, 5229−5237.
11. Banno, Y. T., Nakashima, T., Kumada, T., Ebisawa, K., Nonomura, Y., and Nozawa, Y. (1992) *J. Biol. Chem. 267*, 6488−6494.
12. Furukawa, K., Fu, W., Li, Y., Witke, W., Kwiatkowski, D. J., and Mattson, M. P. (1997) *J. Neurosci. 17*, 8178−8186.
13. Arcaro, A. (1998) *J. Biol. Chem. 273*, 805−813.
14. Azuma, T., Witke, W., Stossel, T. P., Hartwig, J. H., and Kwiatkowski, D. J. (1998) *EMBO J. 17*, 1362−1370.
15. Burtnick, L. D., Koepf, E. K., Grimes, J., Jones, E. Y., Stuart, D. I., McLaughlin, P. J., and Robinson, R. C. (1997) *Cell 90*, 661−670.
16. Yu, F. X., Sun, H. Q., Janmey, P. A., and Yin, H. L. (1992) *J. Biol. Chem. 267*, 14616−14621.
17. Janmey, P. A., Lamb, J., Allen, P. G., and Matsudaira, P. T. (1992) *J. Biol. Chem. 267*, 11818−11823.
18. Yin, H. L., Iida, K., and Janmey, P. A. (1988) *J. Cell Biol. 106*, 805−812.
19. Tuominen, E. K. J., Holopaineu, J. M., Chen, J., Prestwich, G. D., Bachiller, P. R., Kinnunen, P. K. J., and Janmey, P. A. (1999) *Eur. J. Biochem. 263*, 85−92.
20. Prestwich, G. D. (1996) *Acc. Chem. Res. 29*, 503−513.
21. Gu, Q.-M., and Prestwich, G. D. (1996) *J. Org. Chem. 61*, 8642−8647.
22. Thum, O., Chen, J., and Prestwich, G. D. (1996) *Tetrahedron Lett. 37*, 9017−9020.
23. Chaudhary, A., Gu, Q.-M., Thum, O., Profit, A. A., Qi, Y., Jeyakumar, L., Fleischer, S., and Prestwich, G. D. (1998) *J. Biol. Chem. 273*, 8344−8350.
24. Profit, A. A., Chen, J., Gu, Q.-M., Chaudhary, A., Prasad, K., Lafer, E. M., and Prestwich, G. D. (1998) *Arch. Biochem. Biophys. 357*, 85−94.
25. Tall, E., Dormán, G., Garcia, P., Runnels, L., Shah, S., Chen, J., Profit, A. A., Gu, Q.-M., Chaudhary, A., Prestwich, G. D., and Rebecchi, M. J. (1997) *Biochemistry 36*, 7239−7248.
26. Edman, P., and Begg, G. (1967) *Eur. J. Biochem. 1*, 80−91.
27. Laemmli, U. K. (1970) *Nature 227*, 680−685.
28. Chen, J., Profit, A. A., and Prestwich, G. D. (1996) *J. Org. Chem. 61*, 6305−6312.
29. Chaudhary, A., Chen, J., Gu, Q. M., Witke, W., Kwiatkowski, D. J., and Prestwich, G. D. (1998) *Chem. Biol. 5*, 273−281.
30. Prestwich, G. D., Dormán, G., Elliott, J. T., Marecak, D. M., and Chaudhary, A. (1997) *Photochem. Photobiol. 65*, 222−234.
31. Prestwich, G. D., Chaudhary, A., Chen, J., Feng, L., Mehrotra, B., and Peng, J. (1999) in *Phosphoinositides: Chemistry, Biochemistry and Biomedical Applications* (Bruzik, K. S., Ed.) Vol. 818, pp 24−37, American Chemical Society, Washington, DC.
32. Mourey, R. J., Estevez, V. A., Marecek, J. F., Barrow, R. K., Prestwich, G. D., and Snyder, S. H. (1993) *Biochemistry 32*, 1719−1726.
33. Mehrotra, B., Elliott, J. T., Chen, J., Olszewski, J. D., Profit, A. A., Chaudhary, A., Mitsunori, F., Mikoshiba, K., and Prestwich, G. D. (1997) *J. Biol. Chem. 272*, 4237−4244.
34. Theibert, A. B., Estevez, V. A., Mourey, R. J., Marecek, J. F., Barrow, R. K., Prestwich, G. D., and Snyder, S. H. (1992) *J. Biol. Chem. 267*, 9071−9079.
35. Hammonds-Odie, L. P., Jackson, T. R., Profit, A. A., Blader, I. J., Turck, C. W., Prestwich, G. D., and Theibert, A. B. (1996) *J. Biol. Chem. 271*, 18859−18868.
36. Sugiura, Y. (1981) *Biochim. Biophys. Acta 641*, 148−159.
37. Flanagan, L. A., Cunningham, C. C., Chen, J., Prestwich, G. D., Kosik, K. S., and Janmey, P. A. (1997) *Biophys. J. 73*, 1440−1447.
38. Toker, A. (1998) *Curr. Opin. Cell Biol. 10*, 254−261.
39. Toker, A., and Cantley, L. (1997) *Nature 387*, 673−676.
40. Pope, B. J., Gooch, J. T., and Weeds, A. G. (1997) *Biochemistry 36*, 15848−15855.
41. McLaughlin, P. J., Gooch, J. T., Mannherz, H. G., and Weeds, A. G. (1993) *Nature 364*, 685−692.
42. Robinson, R., Mejillano, M., Le, V., Burtnick, L., Yin, H., and Choe, S. (1999) *Science 286*, 1939−1942.
43. McGough, A. (1998) *Curr. Opin. Struct. Biol. 8*, 166−176.
44. Rao, V. D., Misra, S., Boronenkov, I. V., Anderson, R. A., and Hurley, J. H. (1998) *Cell 94*, 829−839.

BI000996Q